

2-7-2018


Estimating Discharge in Low-Order Rivers With High-Resolution Aerial Imagery

Tyler V. King
Utah State University

Bethany T. Neilson
Utah State University

Mitchell T. Rasmussen
Utah State University

Follow this and additional works at: https://digitalcommons.usu.edu/water_pubs

 Part of the [Earth Sciences Commons](#), and the [Water Resource Management Commons](#)

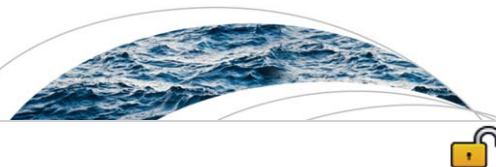
Recommended Citation

King, Tyler V.; Neilson, Bethany T.; and Rasmussen, Mitchell T., "Estimating Discharge in Low-Order Rivers With High-Resolution Aerial Imagery" (2018). *Publications*. Paper 147.

https://digitalcommons.usu.edu/water_pubs/147

This Article is brought to you for free and open access by the Utah Water Research Laboratory at DigitalCommons@USU. It has been accepted for inclusion in Publications by an authorized administrator of DigitalCommons@USU. For more information, please contact digitalcommons@usu.edu.





RESEARCH ARTICLE

10.1002/2017WR021868

Estimating Discharge in Low-Order Rivers With High-Resolution Aerial Imagery

Tyler V. King¹ , Bethany T. Neilson¹ , and Mitchell T. Rasmussen¹¹Utah Water Research Laboratory, Department of Civil and Environmental Engineering, Utah State University, Logan, Utah, USA

Key Points:

- Channel bathymetry was photogrammetrically derived from aerial imagery
- River discharge was estimated by coupling aerial imagery with a 1-D hydraulic model
- Minimal knowledge of the system was required to remotely sense river discharge

Correspondence to:

T. V. King,
tylerking@aggiemail.usu.edu

Citation:

King, T. V., Neilson, B. T., & Rasmussen, M. T. (2018). Estimating discharge in low-order rivers with high-resolution aerial imagery. *Water Resources Research*, 54. <https://doi.org/10.1002/2017WR021868>

Received 14 SEP 2017

Accepted 12 JAN 2018

Accepted article online 18 JAN 2018

Abstract Remote sensing of river discharge promises to augment in situ gauging stations, but the majority of research in this field focuses on large rivers (>50 m wide). We present a method for estimating volumetric river discharge in low-order (<50 m wide) rivers from remotely sensed data by coupling high-resolution imagery with one-dimensional hydraulic modeling at so-called virtual gauging stations. These locations were identified as locations where the river contracted under low flows, exposing a substantial portion of the river bed. Topography of the exposed river bed was photogrammetrically extracted from high-resolution aerial imagery while the geometry of the remaining inundated portion of the channel was approximated based on adjacent bank topography and maximum depth assumptions. Full channel bathymetry was used to create hydraulic models that encompassed virtual gauging stations. Discharge for each aerial survey was estimated with the hydraulic model by matching modeled and remotely sensed wetted widths. Based on these results, synthetic width-discharge rating curves were produced for each virtual gauging station. In situ observations were used to determine the accuracy of wetted widths extracted from imagery (mean error 0.36 m), extracted bathymetry (mean vertical RMSE 0.23 m), and discharge (mean percent error 7% with a standard deviation of 6%). Sensitivity analyses were conducted to determine the influence of inundated channel bathymetry and roughness parameters on estimated discharge. Comparison of synthetic rating curves produced through sensitivity analyses show that reasonable ranges of parameter values result in mean percent errors in predicted discharges of 12%–27%.

1. Introduction

River discharge records are central to fundamental understanding of hydrologic processes. While in situ gauging stations are considered the most accurate approach for estimating river discharge, they are expensive to maintain and in many cases the sites and resulting data can be technically, logistically, and politically difficult to access (Fekete & Vörösmarty, 2007). The limitations of and global decline in in situ gauging stations have given rise to estimation of river discharge from remotely sensed hydraulic variables as a means to augment and extend in situ gauging-station networks (Alsdorf & Lettenmaier, 2003; Dingman & Bjerklie, 2006; Smith et al., 1996).

A wide range of techniques have been developed to estimate discharge from remotely sensed hydraulic variables including substituting remotely sensed stage or width observations for in situ observations at established gauging stations (e.g., Kouraev et al., 2004; Smith, 1997), quantitative imagery analysis (e.g., Johnson & Cowen, 2016; Legleiter et al., 2017; Stumpf et al., 2016), and coupling remotely sensed observations of wetted width, water surface elevation, and/or free surface slope with well-established open-channel flow equations (e.g., Bjerklie et al., 2003; Durand et al., 2014; Garambois & Monnier, 2015; Liu et al., 2015; Wilson et al., 2015). This last approach has received the most attention and is seen as the most applicable to remote, ungauged basins given the potential to use only remotely sensed data products to estimate discharge.

One of the largest impediments to remote sensing of discharge is the need for estimates of channel bathymetry. A wide range of techniques have been proposed to develop empirical correlations between spectral properties and observed water depths (Legleiter et al., 2004, 2009; Lyzenga, 1981; Su et al., 2008; Westaway et al., 2003). These approaches, however, require known depths for calibration and relatively low turbidity in order for light to penetrate the water column and reflect off the river bed. Green LiDAR and

© 2018. The Authors.

This is an open access article under the terms of the Creative Commons Attribution-NonCommercial-NoDerivs License, which permits use and distribution in any medium, provided the original work is properly cited, the use is non-commercial and no modifications or adaptations are made.

radar can be used to map inundated bathymetry in shallow (<2 m deep) waters but require highly specialized and expensive payloads and/or platforms that have prevented widespread adoption (Bailly et al., 2010; Hilldale & Raff, 2008; Melcher et al., 2002). A number of approaches have been presented where channel bathymetry and slope are estimated from the assimilation of river width, slope, and/or water surface elevation with hydrologic modeling (Biancamaria et al., 2011; Durand et al., 2008, 2010, 2014; Mersel et al., 2013; Yoon et al., 2012, 2016); however, these methods often use hydrologic models to provide initial estimates of discharge from ancillary hydrometeorological observations which are not always available in remote locations. As a result, channel bathymetry is often treated as (1) available from an outside source, which may be true for large, socially and economically important water ways (e.g., Pan et al., 2016), but is unlikely for smaller, remote rivers, (2) a set of calibration parameters that are estimated in conjunction with discharge using data assimilation techniques and assumptions about mass conservation over large (10 km) spatial scales (e.g., Durand et al., 2014, 2016; Garambois & Monnier, 2015), or (3) terms to be integrated into a simplified longitudinal trend in hydraulic geometry within the at-many-stations hydraulic geometry framework of Gleason and Smith (2014). For each approach there are trade-offs between accuracy, a priori data requirements, and the scale at which the method can be applied.

The vast majority of reported techniques for remote sensing of discharge have utilized satellite observations with the goal of obtaining global coverage. While these satellite-based approaches have the potential to greatly expand coverage of river discharge estimates (e.g., Pavelsky et al., 2014), their applicability is limited to larger rivers where widths are greater than 100 m. Lower-order river reaches that fall below the width threshold imposed by the resolution of satellite observations are not only ubiquitous (Allen & Pavelsky, 2015; Downing et al., 2012) but are also biogeochemically important (e.g., Ågren et al., 2007), provide critical aquatic habitat (e.g., Rosenfeld et al., 2002), and have the lowest coverage of in situ gauging stations (Pavelsky et al., 2014). As such, alternative methods to in situ gauging stations and satellite-based remote sensing approaches are necessary to quantify discharge and answer basic hydrologic questions within these smaller basins.

In contrast to the coarse resolution of satellite observations used for the extraction of hydraulic properties at global scales, high-resolution imagery has been used for decades to produce digital terrain models of noninundated river channels using photogrammetric techniques (Collin & Chisholm, 1991; Lane et al., 1994). Recent advances in hardware (cameras, platforms, global positioning systems, and inertial momentum units) and postprocessing software have greatly advanced the use of aerial photography for high-resolution three-dimensional reconstruction of noninundated geomorphic units (e.g., Flener et al., 2013; Javernick et al., 2014; Watanabe & Kawahara, 2016). These studies demonstrate the accuracy of extracting digital surface models (DSMs) of river banks from aerial imagery, but stop short of integration with hydraulic modeling to estimate river discharge.

To address the need for and lack of gauging stations in lower-order rivers, we present a technique to estimate river discharge in lower-order rivers that uniquely combines the techniques of extracting channel morphology from high-resolution aerial imagery and estimating river discharge using well-established open-channel flow hydraulics. Our technique builds upon previous approaches of remote sensing of river discharge while taking advantage of the high-resolution information that is available with aerial imagery to estimate river discharge in portions of the watershed that are unobservable with satellite-based observations. With a case study from the Kuparuk River in Arctic Alaska, we take advantage of the properties of Arctic hydrology and geomorphology to demonstrate the feasibility of this method.

2. Methods

With the objective of estimating river discharge remotely, the following general approach was adopted. Aerial surveys were conducted from which wetted widths and channel bathymetry were extracted. Open-channel hydraulic routing models were created for locations identified as virtual gauging stations using the extracted bathymetry. The hydraulic models were used to estimate discharge required to reproduce the wetted widths observed in the aerial imagery. These modeled discharges and extracted widths were used to develop synthetic width-discharge rating curves. In situ observations were then used to determine the accuracy of this approach, as detailed in the following sections.

2.1. Study Site

This method was developed and tested for a 35 km long study reach near the headwaters of the Kuparuk River basin, Alaska (Figure 1). The hydrologic regime is typical of basins over continuous permafrost with flows that are dominated by snowmelt in the spring and rapid responses to precipitation events throughout the summer (Figure 2; McNamara et al., 1998). Top-down thawing of soils in the basin through the summer

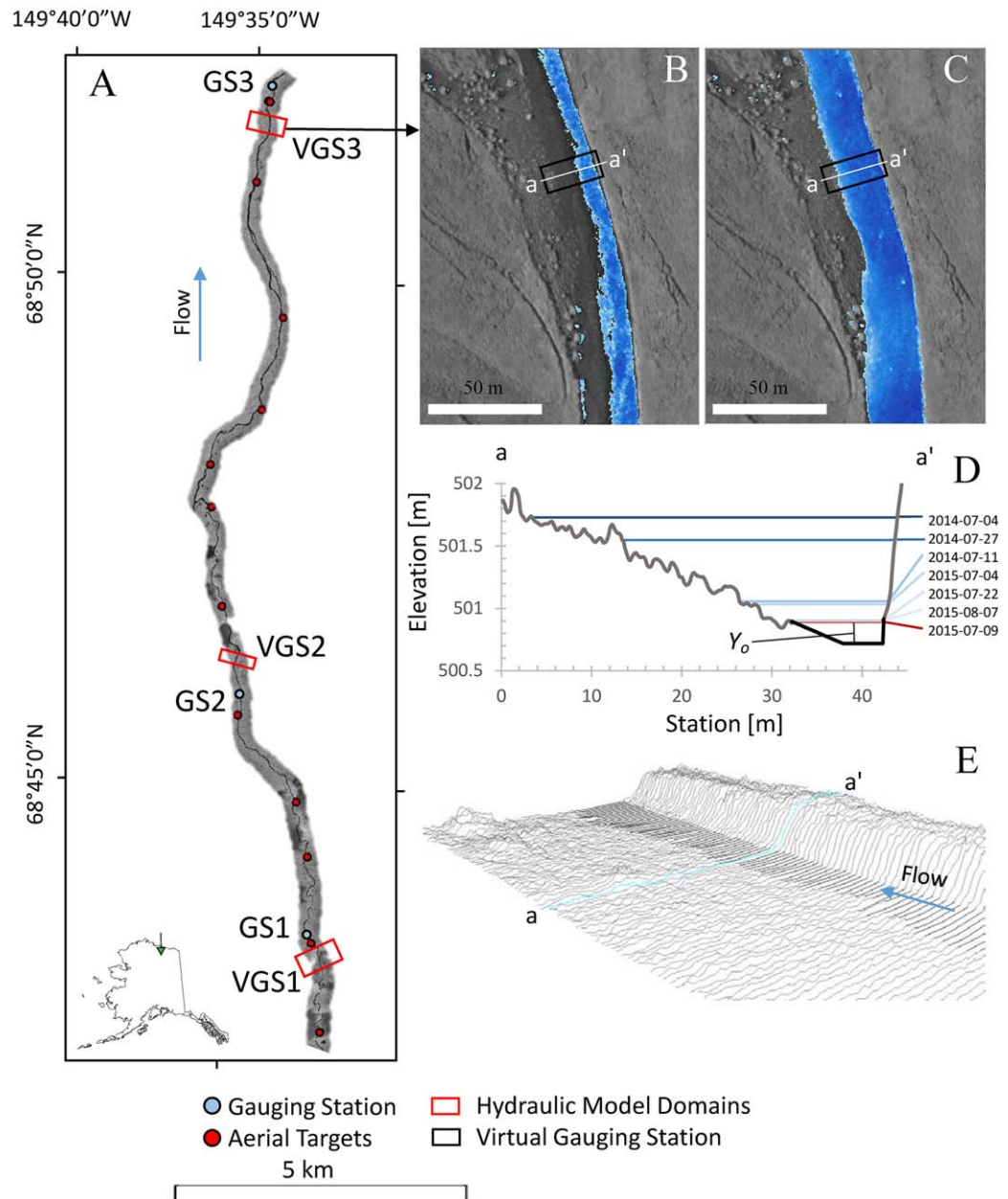


Figure 1. (a) A 22 km portion of a 35 km study reach where hydraulic models were developed for regions (red boxes) that encompassed the three virtual gauging station (black boxes in b and c). Wetted widths were extracted from NIR imagery for each aerial survey and were seen to vary significantly between (b) low and (c) high flows. Exposed channel bathymetry was photogrammetrically extracted under low flows (grey lines in d and e) and bathymetry of the inundated portion of the channel (black lines in d and e) was approximated with trapezoidal channel bathymetry using bank slopes extracted from the adjacent exposed channel topography. Note that the exposed channel under low flows (down to the red line in d) was inundated during subsequent aerial surveys (blue lines in d). Channel bathymetry was determined for all transects (e) in the hydraulic model domains and discharge required to produce extracted widths within the virtual gauging station for each aerial survey was determined using a one-dimensional hydraulic routing model.

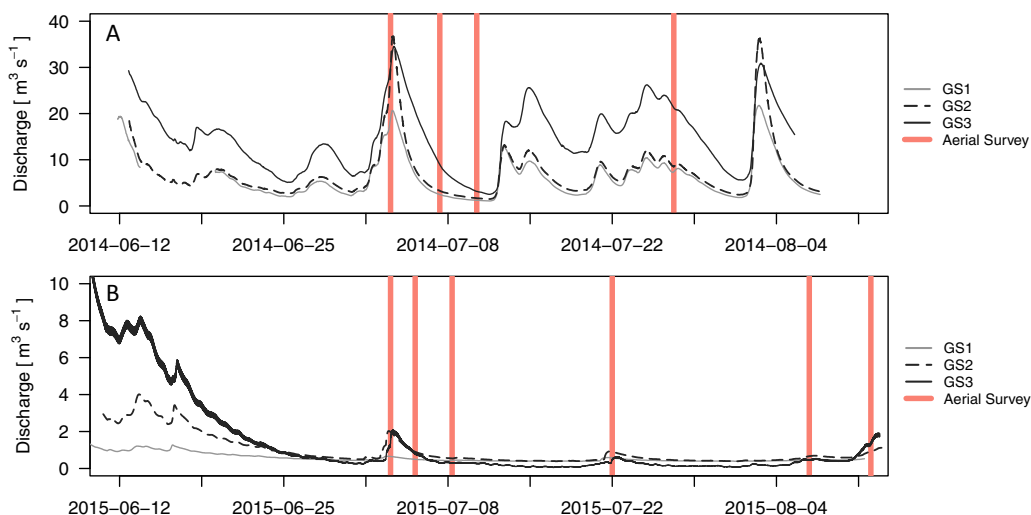


Figure 2. Observed discharge and dates of aerial surveys (vertical colored lines) for (a) 2014 and (b) 2015. Note different y axis scales between years. Aerial surveys were distributed over a wide range of flows and antecedent conditions, with some flights occurring under similar flows at some locations. Imagery from 9 July 2015 was used to extract channel bathymetry.

months only thaws the top tens of centimeters, producing a very thin hydrologically active subsurface layer, or “active layer,” which is bounded underneath by effectively impermeable frozen soil. Limited storage in the active layer produces high runoff/rainfall ratios, rapid and significant rises in streamflow in response to precipitation events throughout the summer months, and recession to very low flows between precipitation events. These discharge regimes, coupled with reaches in the cobble lined alluvial channel with low angle transverse bed slopes, allow for extensive bed exposure under low flows and substantial expansion and contraction in wetted width in response to changes in discharge. A lack of overhanging vegetation allows these changes in width to be observable from above. More details on the Kuparuk River basin are provided in King et al. (2016).

2.2. Data Collection

Virtual gauging stations (VGSs) are locations within river reaches where discharge is related to a remotely sensed attribute (e.g., wetted width) of the inundated river channel. With a goal to establish VGSs in river reaches by combining remotely sensed bathymetry, wetted widths, and hydraulic modeling, we conducted repeat field campaigns and aerial surveys along a 35 km long reach of the Kuparuk River (Figure 1a). Data collection included aerial surveys over a range of discharges to provide high-resolution visible (RGB) and near infrared (NIR) imagery, and in situ observations to evaluate method accuracy.

Aerial imagery was collected from a custom imagery acquisition payload constructed by AggieAir™ at Utah State University. The battery powered payload was mounted to the outside a Robinson R-44 helicopter (Torrance, CA) and controlled wirelessly by an operator within the aircraft. Position, trajectory, and imagery data were collected simultaneously with a fully integrated VectorNav GPS (Dallas, TX), inertial measurement unit, and image acquisition system. RGB imagery was collected with a Canon S-95, which has a 10 megapixel CCD sensor with 8 bit radiometric resolution and ISO range of 80–3,200. NIR imagery was collected with a camera identical to that used for RGB imagery, with the notable exception that the manufacturer’s optical filter was replaced with a Wratten 87 NIR filter, which selects for 750 nm radiation.

Twelve pairs of aerial targets were placed along the river corridor to provide validation of the orthomosaic production. The targets, produced with a quarter-square triangle pattern, were constructed from black and white acrylic sheeting to provide strong brightness contrast. Targets were at least 50 cm by 50 cm, or approximately 3.5 pixels square. For verification purposes, target locations were determined with Trimble R7 (Sunnyvale, CA) survey grade GPS units operated in Fast Static mode and postprocessed with a network adjustment from two continuously operating reference station sites. It should be noted that while aerial

targets are useful for verifying accurate orthorectification, they were not used in the production of the orthorectified mosaics and are therefore not required for method application.

In situ gauging stations located 13, 20, and 35 km along the study reach were developed. These stations were installed for the summer months of June, July, and August, as the remote nature of these sites precluded construction of year-round infrastructure capable of withstanding the winter ice cover and spring breakup. At each location steel posts were driven at least 50 cm into the river bed to which Campbell Scientific CS-450 (Logan, UT) pressure transducers were mounted vertically within perforated PVC cages to diffuse any velocity head. The pressure transducers were mounted near the river bed to allow for measurement of stage under low flow conditions. Periodic discharge measurements were made throughout the periods of pressure transducer deployment using a SonTek FlowtrackerTM (San Diego, CA) handheld Acoustic Doppler Velocimeter for wadable conditions and a Teledyne RD Instruments[®] StreamProTM (Poway, CA) Acoustic Doppler Current Profiler for higher flows. A Trimble M3 (Sunnyvale, CA) total station was used to survey water surface elevation and local benchmarks to relate stage readings between deployments. Rating curves were derived using power law relationships from discharge and corresponding stage observations. Near continuous (15 min) hydrographs were produced from the observations of stage throughout the period of pressure transducer deployment (Figure 2).

Transects between aerial targets were surveyed with a total station to produce ground truthing observations of channel shape. Surveys included targets, vegetated riparian zones, dry river banks, and inundated channels with observations made at locations with significant breaks in slope. Ground surface elevations were recorded which in some cases are up 1.5 m lower than the crown of the vegetation canopy. In these cases, elevations extracted from the photogrammetric DSM are higher than elevations from the total station surveys. This only becomes important for overbank flooding conditions, which this method is not intended to address.

Wetted widths were measured manually between pairs of aerial targets by either pulling a fiberglass tape measure across the river from bank to bank, or by using a Laser Technology TruPulse[®] 360r (Centennial, CO) laser range finder with a flat, broad plastic target held at the edge of water. Measurements were taken in triplicate and mean values used to evaluate the wetted widths extracted from aerial imagery.

2.3. Image Processing

Agisoft PhotoScan was used to produce orthomosaics from NIR imagery for all flights and photogrammetric DSMs from RGB imagery from the flight that corresponded to the lowest flows. Payload positioning information was ingested from on board GPS and IMU units, and point clouds were generated using feature-matching and bundle adjustment. Orthomosaics were produced by spatially averaging the brightness values within the point cloud while pairwise depth map computation algorithms were applied to the point cloud to produce photogrammetric DSMs (Agisoft, 2017).

Wetted widths extracted from the NIR orthomosaics were used to provide the spatial and flow-dependent metric that was then used to select VGS locations and evaluate discharge using the hydraulic model. Note that while water surface elevation could have been used as the observed property in our VGSs, photogrammetric extraction of turbulent water surface elevations are highly inaccurate (Han & Endreny, 2014). Wetted widths were determined by (1) producing orthomosaics from NIR aerial imagery, (2) extracting water masks from the orthomosaics with a binary NIR digital number threshold set manually to coincide with a local minima within the brightness histogram interpreted as the brightness of the narrow margin of wet soil along the water's edges to compensate for incident light conditions, (3) manually extracting a river centerline and producing transects perpendicular to the river centerline at 1 m intervals, and (4) determining the length of each transect intersecting the water mask. Wetted widths extracted from NIR orthomosaics were evaluated against ground-based observations of wetted widths as described below.

Channel bathymetry for the exposed portion of the channel was extracted from the photogrammetrically derived DSM created from RGB imagery collected under the lowest observed flows. Bathymetry of the shallow inundated portion of the river channel was approximated with trapezoidal cross sections using side slopes extracted from the DSM. Bank slopes perpendicular to and within a few meters of the water's edges were extended into the inundated regions until they either intersected the opposite bank

or reached an maximum depth below the lowest observed water surface (d , Figure 1d). An initial guess for d was set at 20 cm for all VGSs based on knowledge of the system and qualitative interpretation of the RGB aerial imagery. The sensitivity of discharge estimates to d was determined as explained below. Limiting the bank slope used in bathymetry extrapolation to within a few meters of the water's edge allowed us to avoid the issues of breaks in bank slope presented in Mersel et al. (2013). The approximated inundated channel bathymetry was merged with the DSM to provide full channel geometry across the floodplain and river channel (Figure 1e). Vertical accuracy of the photogrammetrically derived DSM was evaluated against total station surveys as described below. Some alternative channel geometry processing methods include assuming rectangular cross sections below the minimum observed water surface or continuing bank slopes until they intersect without a maximum depth. The former does not provide unique width under low flows which would provide no lower limit to flows, while the latter produces unstable hydraulic results where localized bank slopes vary significantly between subsequent cross sections.

2.4. Hydraulic Modeling

As described above, VGS locations were selected where a wide range of wetted widths were observed. A subset of three potential locations near aerial targets and in situ gauging stations were selected to test and validate our method for estimating discharge. Hydraulic models of river reaches that encompassed the selected VGSs were produced in HEC-RAS 5.03 (Brunner, 2016) and run with steady state, subcritical flow routines. The downstream water surface elevations were extracted from the DSM for each flight as the elevation at the water mask's edge, similar to the method used in Durand et al. (2014). Hydraulic model domains had transects spaced every meter and the VGSs were located away from the downstream boundary of the model domains to minimize influences from the downstream boundary condition.

Discharge within each hydraulic model domain was estimated for each aerial survey by varying flow in the 1-D hydraulic model until the wetted widths extracted from the NIR orthomosaics were reproduced by the model at the VGSs. Hydraulic simulations were run to ensure that actual discharge values were within the tested flows. For each tested flow, root mean square errors were calculated to compare simulated and extracted wetted widths for transects within the VGSs (wetted width RMSE). The simulated discharge that produced the minimum wetted width RMSE for a given flight was selected as the optimum simulated discharge. To determine the accuracy of this approach, the optimum simulated discharges were evaluated against in situ gauging-station discharges. The precision of this method is determined by comparing results from repeat aerial surveys under similar flow conditions.

In order to take advantage of well-established relationships between width and discharge, known as hydraulic geometries (Leopold & Maddock, 1953), power law width-discharge rating curves were produced for each VGS using widths extracted from imagery and flows that were either estimated from the hydraulic model (synthetic rating curves) or observed at in situ gauging stations (observed rating curves). The production of rating curves allows for discharge to be estimated at each location given only observations of wetted width, and for the identification of ranges in width or discharge for which the simulated and observed regressions are significantly different. To determine if the simulated and observed rating curves were significantly different, 95% confidence intervals were produced for each rating curve. Regions of the curves with overlapping confidence intervals were considered to not be significantly different.

2.5. Accuracy Assessment

Ground-based observations provide the data necessary to evaluate the accuracy of wetted widths extracted from orthomosaics, extracted channel bathymetry, and estimated river discharge. Accuracy of extracted wetted widths was evaluated as absolute error in meters:

$$EB_{i,j} = \sqrt{(B_{obs,i,j} - B_{ext,i,j})^2} \quad (1)$$

where $EB_{i,j}$ is the wetted width absolute error for VGS i for flight j , $B_{obs,i,j}$ is the wetted width for VGS i for flight j measured on the ground, and $B_{ext,i,j}$ is the wetted width for VGS i for flight j extracted from orthomosaics. Percent width error is calculated from absolute error as

$$PEB_{i,j} = \frac{\sqrt{(B_{obs,i,j} - B_{ext,i,j})^2}}{B_{obs,i,j}} \times 100 \quad (2)$$

where $PEB_{i,j}$ is the percent wetted width error for VGS i for flight j . The accuracy of simulated wetted widths was evaluated against the extracted wetted widths with a root mean square error (RMSE) objective function as

$$RMSE_{i,j,k} = \sqrt{\frac{\sum_{m=1}^{n_i} (B_{ext,i,j,m} - B_{mod,i,j,k,m})^2}{n_i}} \quad (3)$$

where $RMSE_{i,j,k}$ is the wetted width root mean square error for VGS i for flight j for tested flow k , $B_{ext,i,j,m}$ is the wetted width for VGS i for flight j for transect m extracted from orthomosaics, $B_{mod,i,j,k,m}$ is the wetted width for VGS i for flight j for tested flow k for transect m produced from the 1-D hydraulic model, and n_i is the number of transects within VGS i .

The photogrammetrically derived DSM (e.g., the portion of the river bed that was exposed under low flows) was compared against total station surveys of transects located between targets. The vertical accuracy was established as the RMSE of elevation between the surveyed and extracted elevations as

$$RMSE_o = \sqrt{\frac{\sum_{p=1}^{q_o} (Z_{obs,o,p} - Z_{ext,o,p})^2}{q_o}} \quad (4)$$

where $RMSE_o$ is the vertical root mean square error for transect o , $Z_{obs,o,p}$ is the elevation of position p on transect o from total station survey, $Z_{ext,o,p}$ is the elevation of position p on transect o extracted from the photogrammetric DSM, and q_o is the number of positions within transect o .

Estimated river discharge from the hydraulic modeling is evaluated against observed river discharge extracted from hydrographs for the given time of each flight using a percent error:

$$PEQ_{i,j} = \frac{Q_{obs,i,j} - Q_{mod,i,j}}{Q_{obs,i,j}} \times 100 \quad (5)$$

where $PEQ_{i,j}$ is the discharge percent error for VGS i for flight j , $Q_{obs,i,j}$ is the discharge observed at the in situ gauging station i for flight j , and $Q_{mod,i,j}$ is the discharge estimated from the hydraulic model that best reproduced the extracted widths for VGS i for flight j . Note that in situ (GS) and virtual (VGS) gauging stations with the same index i are located in close proximity to each other (Figure 1a).

2.6. Sensitivity Analysis

Sensitivity to model parameters of d used in bathymetry estimation and n used in hydraulic modeling were evaluated as percent differences between extracted rating curves and simulated rating curves produced from using plausible ranges of parameter values. Percent errors were calculated by (1) prescribing a reasonable range of n values from published tables (Arcement & Schneider, 1989) and a reasonable range of possible reach averaged d determined from visual inspection of the high-resolution aerial imagery, (2) routing ranges of discharge through the 1-D hydraulic models for all combinations of reasonable depth and roughness values, (3) determining simulated discharge values that best reproduced the widths extracted for each simulation, (4) producing power law discharge-width rating curves from the simulation results, and (5) calculating the percent errors between simulated and extracted rating curves for the region where there is significant difference in the curves for each simulation run (equation (6)).

$$\overline{PEQ}_{n,d,i} = \left| \frac{\sum_{w=w_{o,i}}^{r_i} \frac{Q_{sim,w,n,d,i} - Q_{obs,w,i}}{Q_{obs,w,i}}}{N_{widths}} \right| \times 100 \quad (6)$$

where $\overline{PEQ}_{n,d,i}$ is the mean percent difference magnitude between observed and simulated discharges for VGS i for the range in width where simulated and extracted rating curves were significantly different for simulations using roughness value of n , and depth of d ; w is the wetted width, $w_{o,i}$ is the statistical significance threshold width for VGS i described above; r_i is the maximum observed width for VGS i ; $Q_{sim,w,n,d,i}$ is the simulated discharge for width w at VGS i using roughness n and depth d above the significance

threshold; $Q_{obs,w,i}$ is the observed discharge for width w at VGS i ; and N_{widths} is the number of simulated widths above the threshold w_i and below the maximum observed width r_i .

Ranges for d and n values were determined to span the range of reasonable values. d was initially set to 20 cm with a range of 10–50 cm based on knowledge of the system and visual inspection of the RGB imagery. Channel roughness (n) was initially set to 0.04 with a range of 0.03–0.05 based on the cobble substrate that is evident in the high-resolution aerial imagery and published literature (Arcement & Schneider, 1989; Barnes, 1967). Irregularities, variations in channel cross section, obstructions, vegetation, and meandering were negligible for these sites, negating the need to modify the base roughness value. Our selection of 0.04 is commensurate with the work of Kane et al. (2003) for the same river.

From these percent error values, sensitivity of discharge estimates were calculated for each VGS in two ways: (1) the mean and standard deviation of percent error magnitudes from varying both depth and roughness (equation (7)) and (2) the mean and standard deviation of the range of percent differences from varying one parameter at a time (equations (8) and (9)). The former provides an estimate of the magnitude of the error associated with the range of both parameters, while the latter provides a measure of the range of the error associated with each parameter.

$$E_i = \frac{\left(\sum_{n=0.03}^{0.05} \left(\sum_{d=10}^{50} (\overline{PEQ}_{n,d,i}) \right) \right)}{N_{depths} * N_{roughnesses}} \tag{7}$$

$$E_{depth,i} = \frac{\left(\sum_{n=0.03}^{0.05} (\overline{PEQ}_{n,d=50,i} - \overline{PEQ}_{n,d=10,i}) \right)}{N_{roughnesses}} \tag{8}$$

$$E_{rough,i} = \frac{\left(\sum_{d=10}^{50} (\overline{PEQ}_{n=0.03,d,i} - \overline{PEQ}_{n=0.05,d,i}) \right)}{N_{depths}} \tag{9}$$

where E_i is the mean percent difference magnitude for VGS i , N_{depths} and $N_{roughnesses}$ are the number of depth and roughness values used in the sensitivity analysis, respectively, and $E_{depth,i}$ and $E_{rough,i}$ are the sensitivity of a VGS i to variations in d and n , respectively.

3. Results

Ten aerial surveys conducted in 2014 and 2015 had average durations of 40 min, were conducted at approximately 300 m above ground at an average ground speed of 17 m s⁻¹ and produced 0.14 m resolution imagery with imagery overlap of 30–40%. Wetted widths extracted from the resulting NIR orthomosaics had a mean accuracy of 0.36 m with a standard deviation of 0.28 m (or 0.36 m ± 0.28 m) when compared against 11 field observations (Table 1). This level of accuracy corresponds with approximately two and a half pixels in the orthomosaics, and 2% ± 1% of the observed wetted widths. Discharge ranged over an order of magnitude at each of the in situ gauging stations across all aerial surveys (Table 2 and Figure 2), producing wetted widths ranging from 8 to 42 m.

Table 1
Difference Between Observed and Extracted Wetted Widths (EB) in Absolute Distance (m) and Percentage (PEB) of Observed Widths (%)

VGS	Date									
	8/7/2015		7/6/2015		7/22/2015		8/12/2015		Mean	
	m	%	m	%	m	%	m	%	m	%
VGS1	NA	NA	0.02	0.2	0.3	3	0.1	1	0.14	1
VGS2	0.3	2	NA	NA	NA	NA	0.5	3	0.40	3
VGS3	0.4	1	NA	NA	0.4	2	0.8	3	0.53	2
Mean	0.35	2	0.02	0.2	0.35	2	0.47	3	0.36	2

Note. NA, observed data not available.

Table 2
Aerial Survey Flight Specifics

Flight #	Date	Resolution (m)	Observed discharge ($\text{m}^3 \text{s}^{-1}$)			Estimated discharge ($\text{m}^3 \text{s}^{-1}$)			Percent error		
			GS1	GS2	GS3	VGS1	VGS2	VGS3	VGS1	VGS2	VGS3
1	2015-07-09	0.18	0.58	0.70	0.29	0.61	0.86	0.30	5	24	3
2	2015-08-07	0.10	0.71	0.81	0.49	0.80	0.85	0.52	13	4	6
3	2015-07-06	0.11	0.72	0.90	0.51	0.81	NA	NA	12	NA	NA
4	2015-07-22	0.15	0.84	0.99	0.51	0.81	1.15	0.52	-4	16	1
5	2015-07-04	0.14	1.40	1.80	1.65	1.37	1.67	1.44	-2	-7	-13
6	2015-08-12	0.10	1.10	1.27	1.73	0.97	1.18	NA	-12	-7	NA
7	2014-07-11	0.15	1.15	1.58	2.78	1.16	1.69	2.78	<1	7	<1
8	2014-07-08	0.17	1.91	2.59	5.69	2.12	2.69	NA	11	-4	NA
9	2014-07-27	0.14	6.91	8.84	18.55	5.74	8.49	17.81	-9	4	-4
10	2014-07-04	0.13	13.95	21.39	38.22	13.11	22.67	38.22	-6	6	<1
	Mean	0.14						Mean	8	9	4
								Grand mean	7 ± 6		

^aNA, imagery not available.

Hydraulic model domains ranging from 53 to 120 m long encompassed the three selected VGS locations and were populated using DSMs produced from RGB imagery collected on 9 July 2015, the flight that corresponds with the narrowest extracted top widths. In these images, the inundated portion of the channel within the VGSs occupied as little as 20% of the wetted widths observed under high flows (Figures 1b and 1c). The photogrammetrically derived DSM captured the shape of the noninundated portion of the channel well and was vertically accurate with an average vertical RMSE of $0.23 \text{ m} \pm 0.05 \text{ m}$ across 37 observations at three transects (Figure 3).

Using our assumed initial parameter values of 20 cm for d and 0.04 for n , remotely sensed estimates of discharge fall within the 95% confidence intervals of the in situ rating curve, showing no statistically significant

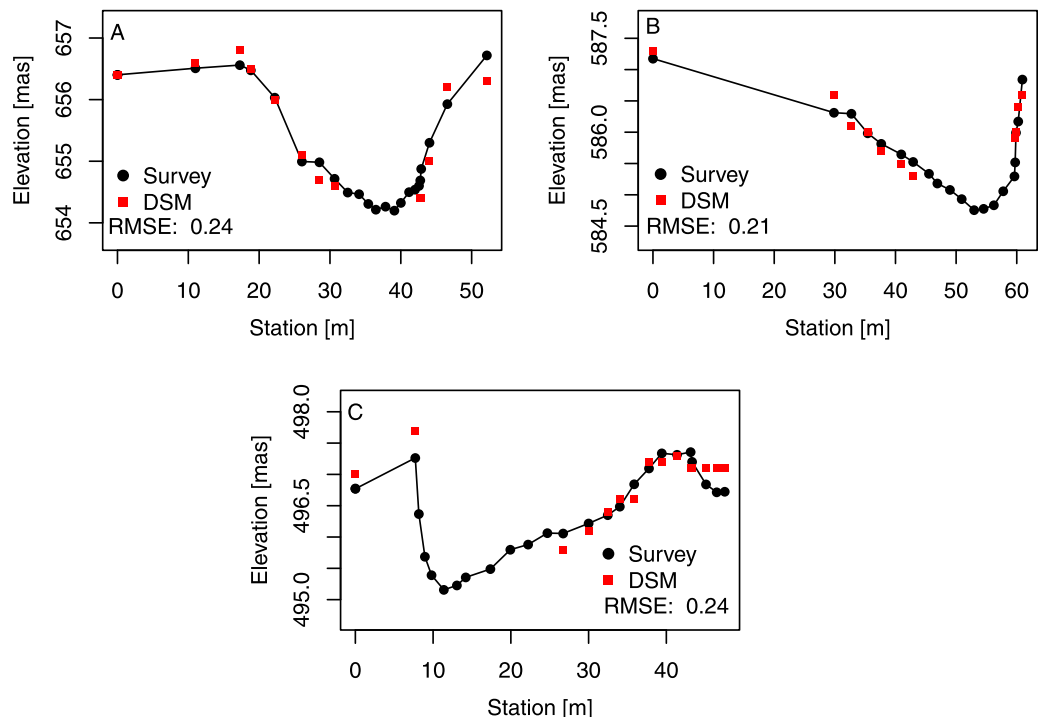


Figure 3. Transect elevation profiles in meters above sea level (mas) from (a) VGS1, (b) VGS2, and (c) VGS3 extracted from the photogrammetric DSM (red squares) and from total station surveys (black circles). Mean vertical RMSE is 0.23 m. Note that displayed DSM values are limited to stations where survey observations are available.

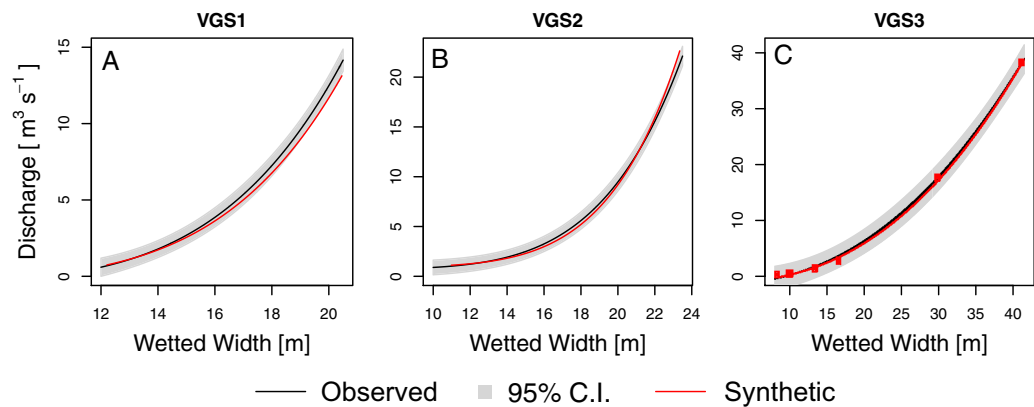


Figure 4. Observed (black lines) and synthetic (red lines) rating curves for (a) VGS1, (b) VGS2, and (c) VGS3. All simulated discharges (red dots) fall within the 95% confidence intervals (grey regions) of the observed rating curves showing that there are no statistically significant differences between the observed and simulated discharges.

differences between the simulated and observed discharges (Figure 4). The mean percent error across all sites and all observed flows was $7\% \pm 6\%$ (Table 2). Repeat flights conducted under similar flow conditions (e.g., 7 August 2015 and 6 July 2015 for VGS1, and 7 August 2015 and 22 July 2015 for VGS3) produced discharge estimates within 5% of each other, indicating that between-flight variation is minimal and that there is a high level of method precision (Table 2).

Statistical significance thresholds from the sensitivity analysis were 15, 16, and 18 m in width for VGS1, VGS2, and VGS3, respectively (Figure 5). Below these widths the extracted and simulated rating curves were not significantly different from each other across all values of d and n . Above these thresholds, the rating curves become significantly different for at least some combinations of assumed parameter values. The mean percent error magnitudes increase to from 8% to $27\% \pm 16\%$ at VGS1, 9% to $25\% \pm 16\%$ at VGS2, and 4% to $12\% \pm 7\%$ at VGS3 (Figure 5). These represent scenarios where only general values for depth and roughness are available. If either depth or roughness values are well constrained, mean percent error magnitudes decrease by one third. This analysis also illustrated that there is a transition in dominant sensitivity with distance downstream (Table 3 and Figure 6). Sensitivity to depth (E_{depth}) decreases and sensitivity to roughness (E_{rough}) remains constant with distance downstream. VGS1 is two times more sensitive to depth ($72\% \pm 4\%$) than roughness ($33\% \pm 6\%$), VGS2 is equally sensitive to depth ($53\% \pm 8\%$) and roughness ($42\% \pm 8\%$), and VGS3 is three times more sensitive to roughness ($31\% \pm 2\%$) than depth ($9\% \pm 3\%$) (Table 3).

4. Discussion

These results demonstrate that our approach of coupling high-resolution aerial imagery with open-channel hydraulic modeling produces remotely sensed estimates of river discharge with accuracy levels that are on par with in situ gauging stations and other remote sensing approaches. Evaluating method performance across different discharges and between sites allows us to suggest conditions and VGS characteristics where this method works best. Percent error in model performance is highest for the bottom 20% of observed flows (Table 2). This is expected as under these low flow conditions the estimated channel bathymetry makes up the majority of the channel cross-sectional area. Discharge estimates are also most accurate for VGS3 which had the greatest flow, the straightest planform, the most consistent river width with distance downstream, and widest ranges in wetted widths. These characteristics likely indicate beneficial traits in potential VGS sites and should be included in the selection of VGS locations. Other factors that could influence successful VGS selection include uniform bank slopes leading to and extending into the wetted portion of the channel and uniform bed forms.

The fundamental approach of estimating river discharge from partial observations of the river channel and estimates of unobservable parameters (e.g., d and n) has received a great deal of attention in recent years (e.g., Durand et al., 2014, 2016; Yoon et al., 2016). Our proposed application of estimating discharge from remotely sensed river widths using VGS rating curves is similar to the early attempts to remotely sense river

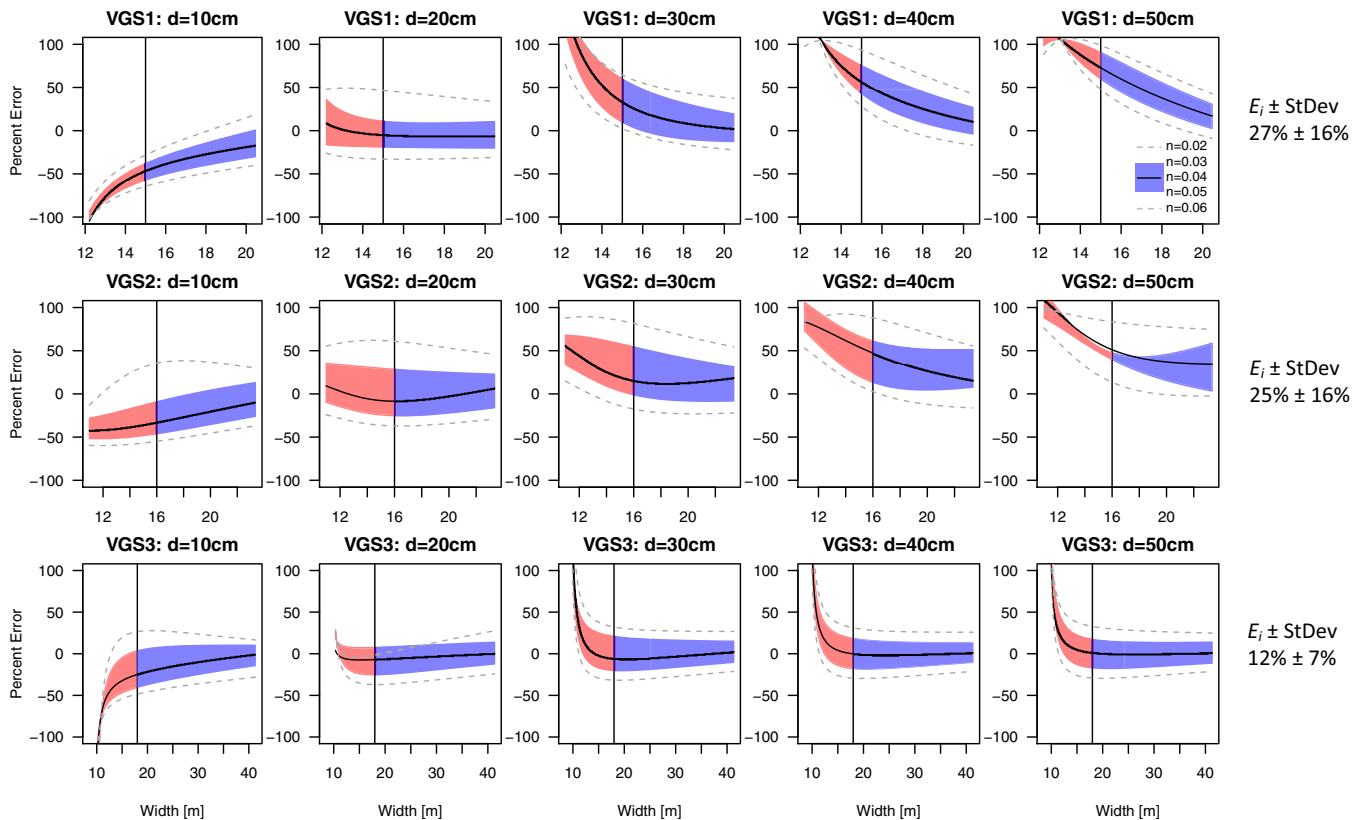


Figure 5. Percent error between simulated and observed rating curves for (top row) VGS1, (middle row) VGS2, and (bottom row) VGS3 grouped by simulated depth (columns). Shaded region shows the range of percent errors for channel roughness values of 0.03 (top of shaded regions), 0.04 (black line), and 0.05 (bottom of shaded regions). Percent error statistics (E_i on right of each set of figures, E_{depth} and E_{rough} in Table 3) are calculated for the statistically significant regions (blue shading right of the vertical lines). The percent errors for roughness values of 0.02 (top dashed grey line) and 0.06 (bottom dashed grey line) are shown for illustrative purposes but are not included in the statistical analysis as these values are outside the reasonable range of representative channel characteristics.

discharge as outlined by Smith (1997) and Kouraev et al. (2004) among others, who used empirical relationships between remotely sensed hydraulic characteristics and ground-based observations of discharge. The notable difference is that our rating curves are produced from hydraulic models derived from remotely sensed data products allowing our approach to be applied to ungauged basins where discharge observations are not available. Estimating inundated channel bathymetry from exposed channel geometry was demonstrated by Mersel et al. (2013) and informed our approach of extending river bank slopes to a maximum depth below the minimum observed water surface. However, in our approach we extract the channel geometry from one low flow flight while the WSE-width pairwise observations method presented in Mersel et al. (2013) requires many repeat observations over the full range of discharges. We further take advantage of the very low flow conditions observed in our lower-order river reach to minimize the area for which bathymetry needs to be estimated. Integrating observations of hydraulic features with hydraulic modeling has also received attention in recent years. For example, Giustarini et al. (2011) and Neal et al. (2009) showed that assimilation of remotely sensed hydrologic features with hydrodynamic models can improve estimates of river discharge given observations of channel bathymetry and a coupled hydrologic-hydraulic modeling framework. However, these approaches often require ancillary data to drive hydrologic models and/or provide bathymetry. Gleason and Smith (2014) made significant advancements in the field of estimating river discharge using only remote sensed observations by utilizing longitudinal trends in hydraulic geometry laws that scale with the range of observed wetted widths. Central to their approach is the assumption of mass conservation over long (10 km) river reaches allowing for parameter calibration using a genetic algorithm to preserve discharge continuity within the modeled reaches. Similarly, the GaMo and MetroMan algorithms presented in Garambois and Monnier (2015) and Durand et al. (2014), respectively, preserve continuity of discharge within study domains in order to estimate cross-sectional area of the channel at zero

Table 3
Percent Error Values (*Italicized Text*) for the Statistically Significant Portions of the Simulated Rating Curves for All Combinations of Depth and Channel Roughness

	Depth	Roughness (%)			Range from varying roughness (%) ^a	$E_{rough}^b \pm StDev$ (%)
		<i>n</i> = 0.03	<i>n</i> = 0.04	<i>n</i> = 0.05		
VGS1	<i>d</i> = 10 cm	-17	-29	-42	25	33 ± 6
	<i>d</i> = 20 cm	10	-6	-20	29	
	<i>d</i> = 30 cm	36	13	-6	42	
	<i>d</i> = 40 cm	49	29	14	35	
	<i>d</i> = 50 cm	59	42	27	32	
	Range from varying depth ^c $E_{depth}^d \pm StDev$	76	71	69		
VGS2	<i>d</i> = 10 cm	3	-21	-36	39	42 ± 8
	<i>d</i> = 20 cm	25	-3	-22	47	
	<i>d</i> = 30 cm	42	14	-7	49	
	<i>d</i> = 40 cm	53	29	7	47	
	<i>d</i> = 50 cm	47	39	19	29	
	Range from varying depth ^c $E_{depth}^d \pm StDev$	45	61	55		
VGS3	<i>d</i> = 10 cm	9	-11	-26	35	31 ± 2
	<i>d</i> = 20 cm	11	-3	-19	30	
	<i>d</i> = 30 cm	17	-3	-16	33	
	<i>d</i> = 40 cm	14	-1	-15	29	
	<i>d</i> = 50 cm	14	0	-15	29	
	Range from varying depth ^c $E_{depth}^d \pm StDev$	5	11	11		

^aMaximum ranges of percent errors resulting from varying channel roughness values for each simulated depth value. ^bSensitivity to variations in roughness defined in equation (9). ^cMaximum ranges of percent errors resulting from varying depth for each simulated roughness value. ^dSensitivity to variations in depth defined in equation (8).

flow and channel roughness using optimization algorithms. Durand et al. (2016) compared these and other approaches to estimate river discharge using some or all of the hydraulic parameters that the forthcoming Surface Water and Ocean Topography (SWOT, <https://swot.jpl.nasa.gov/>) satellite mission is expected to provide. This highly anticipated satellite mission promises to provide wetted width, water surface elevation, and slope for river reaches over 10 km long and 100 m wide with the possibility of reducing the threshold of observable widths down to 50 m (Fu et al., 2012). Pavelsky et al. (2014) estimated the potential impact of

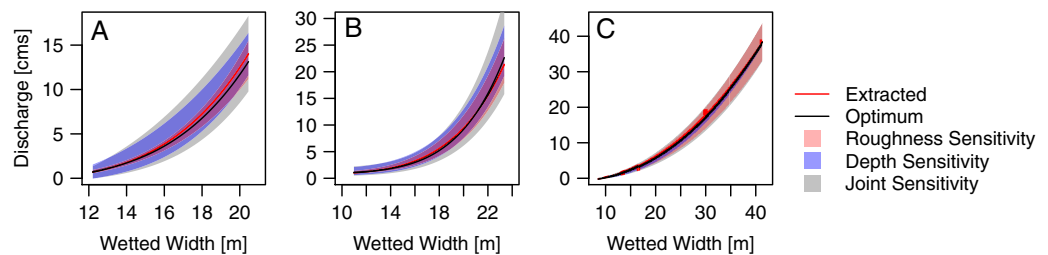


Figure 6. Discharge-width power law rating curves for (a) VGS1, (b) VSG2, and (c) VGS3. Extracted rating curves (red lines) reflect observed discharges versus extracted widths, and optimum rating curves (black lines) reflect simulated discharges versus simulated widths using a maximum depth of 20 cm and roughness of 0.04. The error bounds on the optimum rating curves reflect the range of rating curves that result from varying depth (blue regions) while holding roughness at 0.04, varying roughness while holding depth at 20 cm (red regions), and varying depth and roughness simultaneously (grey regions).

estimating discharge globally for all rivers down to these two potential observability thresholds and determined that both levels of observation will greatly increase coverage compared with the fraction of basins observed by gauges in the Global Runoff Data Centre (GRDC) network. In their analysis, Pavelsky et al. (2014) illustrated a case where smaller observations thresholds were required to disaggregate upstream signals into the contributing basins. Our work is a direct continuation of this line of reasoning by further reducing the threshold of detection through the use of high-resolution data products.

Using high-resolution observations allows us to estimate discharge for reaches on the order of 100 m in length as opposed to the 10 km length required in the satellite-based algorithms. This level of granularity is required to identify hydrologically significant processes in lower-order rivers. For example, discharge records from the in situ gauges in the Kuparuk River show that the GS1-GS2 reach is continuously a gaining reach, but that the GS2-GS3 reach is a losing reach for the five lowest flow flights and a gaining reach for the five highest flow flights (Figures 1a and 2 and Table 2). These longitudinal trends were identified in the remote sensing discharge estimates (Table 2), illustrating the utility of distributed estimates to detect spatial trends in discharge which impacts longitudinal chemical and thermal responses. Further, the establishment of additional VGSs within the study domain could be used to better constrain lateral inflow trends including identifying transition zones between gaining and losing reaches, estimating discharge from surface water sources by differencing VGSs that bracket sources, and estimating net groundwater influences by differencing VGSs within a reach with no visible surface water sources.

Arctic tundra landscapes provide a compelling need for the presented method given the lack of in situ gauging stations at high latitudes (Lammers et al., 2001) and the need for better understanding of runoff generation processes contributing to the observed increases in discharge to the Arctic Ocean (Fu et al., 2012; McClelland et al., 2006; Peterson et al., 2002). However, we suggest this method may be applicable to other systems where three basic requirements are met (1) low flow conditions where a significant portion of the river bed is exposed, (2) a clear nadir view of the channel from above, and (3) a wide range of wetted widths in response to discharge. A large fraction of Arctic, Antarctic, alpine, ephemeral, and desert rivers meet these criteria due to extended low (or no) flow periods, minimal overhanging vegetation, and large fluctuations in flow. Similar conditions also exist in streams and rivers where significant agricultural withdrawals dewater channels (e.g., Western United States), providing a clear management application for this method. Additional testing across multiple systems is required, and we acknowledge that the proposed method is not applicable in all river systems. However, no single solution exists for the challenge of remotely sensing discharge and the approach presented here is intended to act as a member in the ensemble of methods, similar to that presented by Durand et al. (2016). Additional testing should also be done to determine if these results can be achieved with high-resolution satellite observations. Doing so may provide a path toward larger spatial coverage and integration with additional sensors, such as altimetry observations, which could be used to develop multiparameter rating curves which could improve method accuracy.

While the sensitivity analysis suggests that reasonable ranges for n and d produce acceptable ranges of discharge estimates, direct observation of these parameters would provide a significant advancement in the field and could make the method applicable to more systems. We suggest two possible paths forward to estimate these parameter values remotely, and one possible direction that could obviate the need to estimate channel roughness altogether. First, channel bathymetry of the inundated portion may be determined by spectral analysis following the techniques first presented by Lyzenga (1981) and demonstrated extensively since then (e.g., Carbonneau et al., 2006; Flener, 2013; Legleiter, 2015; Legleiter et al., 2004, 2009; Lyon et al., 1992; Marcus et al., 2003; Su et al., 2008). We propose that by using the regions of the riverbed that are exposed under low flow conditions and inundated under high flow conditions to calibrate the empirical relationship between depth and spectral properties, the need for in situ observations of channel depth may be eliminated. Producing full channel geometry by merging dryland topography extracted photogrammetrically with inundated bathymetry approximated with spectral analysis is not a novel idea (e.g., Flener et al., 2013; Javernick et al., 2014; Westaway et al., 2003). However, the approaches to date have required in situ observations of depth for model calibration while our suggestion is based solely on remotely sensed data products. Second, analysis of the three-dimensional point cloud that is produced as an intermediate product in the photogrammetric processing may provide estimates of channel roughness as suggested by Butler et al. (1998). While this has not been done from aerial imagery, Vetter et al. (2011)

have demonstrated this concept with a point cloud collected with airborne laser scanning. It is unclear what resolution and accuracy is needed for analysis of the point cloud to accurately represent the channel roughness, and this should be the focus of additional research. Lastly, known difficulty in assigning channel roughness a priori has been addressed through development of conveyance routines that do not include channel roughness (e.g., Dingman & Sharma, 1997; Jarrett, 1984; López et al., 2007; Riggs, 1976). While these methods obviate the need to estimate channel roughness, they require estimation of fitting parameters which are often derived from regression analysis of large data sets. Future work could focus on integrating these alternative conveyance methods with the method presented here to reduce the dependency on accurate estimates of channel roughness, especially if fitting parameters can be related to remotely sensed physical characteristics.

5. Conclusions

In a time of gauging-station decline and increased hydrologic variability, there is need for methods that provide accurate estimates of river discharge via remote sensing with minimal a priori information. Satellite-based discharge algorithms are being developed to provide estimates of discharge for rivers above approximately 50–100 m wide. However, this technologically derived threshold holds little hydrologic significance and will exclude large and functionally important portions of drainage networks. We propose a method for remotely sensing river discharge for lower-order rivers by coupling high-resolution overlapping aerial imagery with hydraulic modeling. Channel geometry exposed under low flow conditions is extracted from high-resolution aerial imagery, leaving a small portion of the river bathymetry to be estimated from the surrounding topography. Wetted widths extracted from repeat aerial imagery under a range of flows are used to identify locations where width varies in response to discharge. Virtual gauging stations were selected as locations that had a strong variation in wetted width in response to discharge. One-dimensional hydraulic models were created for three locations with which synthetic rating curves were created. Discharge may be estimated from these synthetic rating curves given only an observation of channel wetted width.

With a mean accuracy of $7\% \pm 6\%$, this method is comparable with in situ measurements of river discharge and other methods of remotely sensing volumetric river discharge. Limitations of this method include the need to estimate channel roughness (n) and maximum channel depth under the lowest observed flow conditions (d). The former can be estimated from the analysis of the substrate visible in the high-resolution aerial imagery, while the latter depends on knowledge of the system and subjective inspection of the imagery. However, sensitivity analyses investigating the influence of these parameters produced mean percent errors in predicted discharges ranging from 12% to 27% over ranges of reasonable assumed d and n values indicating that even a general estimate of these parameters produces reasonably accurate estimates.

We have tested and developed this method across multiple locations within an Arctic tundra watershed, and found that there are three basic requirements for method application: (1) low flow conditions that expose substantial portions of the river bed, (2) a clear nadir view of the entire river including the water's edge (e.g., lack of overhanging riparian vegetation), and (3) geomorphic features that provide a wide range of widths as a function of discharge. Testing of this method across more and different channel types should be undertaken to determine the range of conditions for which this method remains applicable, however, most Arctic, Antarctic, alpine, desert, and ephemeral streams meet the method requirements identified.

Through the development of accurate spatially average discharge-width rating curves (virtual gauging stations), there is a clear opportunity to couple this approach with high-resolution satellite imagery to provide regular estimates of river discharge, even if these data products are not capable of extracting channel bathymetry with the accuracy of aerial imagery. This method provides an opportunity to extend gauging-station networks to ungauged rivers that are often inaccessible for technical, logistical, and political reasons and to densify existing gauging-station networks to quantify lateral inflows (e.g., groundwater exchanges and surface water contributions/abstractions) between in situ gauging stations. While the proof of concept used aerial imagery, this method could be used with high-resolution satellite imagery to provide global coverage.

Acknowledgments

Financial support for this work was provided by the National Science Foundation (OPP 1204220, DEB 1026843) and Utah State University through the Utah Water Research Laboratory. The authors extend special thanks to L. Overbeck, D. Kane, J. Homan, R. Gieck, R. Fulweber, J. Stuckey, J. Noguera, M. Winkelaar, A. Jensen, S. Syrstad, and numerous anonymous reviewers. Data and models used in this work are available online at <https://doi.org/10.4211/hs.9badb941303d4813b3c398cdab038368>.

References

- Agisoft. (2017). *Agisoft PhotoScan User Manual: Professional Edition. Version 1.3*. Saint-Petersburg, Russian Federation: Agisoft LLC.
- Ågren, A., Buffam, I., Jansson, M., & Laudon, H. (2007). Importance of seasonality and small streams for the landscape regulation of dissolved organic carbon export. *Journal of Geophysical Research: Biogeosciences*, *112*, G03003. <https://doi.org/10.1029/2006JG000381>
- Allen, G. H., & Pavelsky, T. M. (2015). Patterns of river width and surface area revealed by the satellite-derived North American River Width data set. *Geophysical Research Letters*, *42*, 395–402. <https://doi.org/10.1002/2014GL062764>
- Alsdorf, D. E., & Lettenmaier, D. P. (2003). Tracking fresh water from space. *Science*, *301*(5639), 1491. <https://doi.org/10.1126/science.1089802>
- Arcement, G. J., & Schneider, V. R. (1989). *Guide for selecting Manning's roughness coefficients for natural channels and flood plains* (Rep. 2339). Reston, VA: U.S. Geological Survey.
- Bailly, J. S., Le Coarer, Y., Languille, P., Stigermark, C. J., & Allouis, T. (2010). Geostatistical estimations of bathymetric LiDAR errors on rivers. *Earth Surface Processes and Landforms*, *35*(10), 1199–1210. <https://doi.org/10.1002/esp.1991>
- Barnes, H. H. (1967). *Roughness characteristics of natural channels* (Vol. vi, 213 pp.). Washington, DC: United States Government Publishing Office.
- Biancamaria, S., Durand, M., Andreadis, K. M., Bates, P. D., Boone, A., Mognard, N. M., et al. (2011). Assimilation of virtual wide swath altimetry to improve Arctic river modeling. *Remote Sensing of Environment*, *115*(2), 373–381.
- Bjerklie, D. M., Dingman, S. L., Vorosmarty, C. J., Bolster, C. H., & Congalton, R. G. (2003). Evaluating the potential for measuring river discharge from space. *Journal of Hydrology*, *278*(1–4), 17–38. [https://doi.org/10.1016/S0022-1694\(03\)00129-X](https://doi.org/10.1016/S0022-1694(03)00129-X)
- Brunner, G. W. (2016). *HEC-RAS, river analysis system hydraulic reference manual* (Comput. Program Doc. Rep. CPD-69, 538 pp.). Davis, CA: US Army Corps of Engineers Hydrologic Engineering Center.
- Butler, J. B., Lane, S. N., & Chandler, J. H. (1998). Assessment of DEM quality for characterizing surface roughness using close range digital photogrammetry. *The Photogrammetric Record*, *16*(92), 271–291. <https://doi.org/10.1111/0031-868X.00126>
- Carbonneau, P. E., Lane, S. N., & Bergeron, N. (2006). Feature based image processing methods applied to bathymetric measurements from airborne remote sensing in fluvial environments. *Earth Surface Processes and Landforms*, *31*(11), 1413–1423. <https://doi.org/10.1002/esp.1341>
- Collin, R. L., & Chisholm, N. W. T. (1991). Geomorphological photogrammetry. *The Photogrammetric Record*, *13*(78), 845–854. <https://doi.org/10.1111/j.1477-9730.1991.tb00752.x>
- Dingman, S. L., & Bjerklie, D. M. (2006). Estimation of river discharge. In *Encyclopedia of hydrological sciences*. Hoboken, NJ: John Wiley.
- Dingman, S. L., & Sharma, K. P. (1997). Statistical development and validation of discharge equations for natural channels. *Journal of Hydrology*, *199*(1–2), 13–35.
- Downing, J. A., Cole, J. J., Duarte, C. M., Middelburg, J. J., Melack, J. M., Prairie, Y. T., et al. (2012). Global abundance and size distribution of streams and rivers. *Inland Waters*, *2*(4), 229–236. <https://doi.org/10.5268/IW-2.4.502>
- Durand, M., Andreadis, K. M., Alsdorf, D. E., Lettenmaier, D. P., Moller, D., & Wilson, M. (2008). Estimation of bathymetric depth and slope from data assimilation of swath altimetry into a hydrodynamic model. *Geophysical Research Letters*, *35*, L20401. <https://doi.org/10.1029/2008GL034150>
- Durand, M., Gleason, C. J., Garambois, P. A., Bjerklie, D., Smith, L. C., Roux, H., et al. (2016). An intercomparison of remote sensing river discharge estimation algorithms from measurements of river height, width, and slope. *Water Resources Research*, *52*, 4527–4549. <https://doi.org/10.1002/2015WR018434>
- Durand, M., Neal, J., Rodriguez, E., Andreadis, K. M., Smith, L. C., & Yoon, Y. (2014). Estimating reach-averaged discharge for the River Severn from measurements of river water surface elevation and slope. *Journal of Hydrology*, *511*, 92–104. <https://doi.org/10.1016/j.jhydrol.2013.12.050>
- Durand, M., Rodriguez, E., Alsdorf, D. E., & Trigg, M. (2010). Estimating river depth from remote sensing swath interferometry measurements of river height, slope, and width. *IEEE Journal of Selected Topics in Applied Earth Observations and Remote Sensing*, *3*(1), 20–31.
- Fekete, B. M., & Vörösmarty, C. J. (2007). *The current status of global river discharge monitoring and potential new technologies complementing traditional discharge measurements*. Paper presented at Predictions in Ungaged Basins: PUB-Kick-off, IAHS Publication, Brasilia, November 20–22, 2002.
- Flener, C. (2013). Estimating deep water radiance in shallow water: Adapting optical bathymetry modelling to shallow river environments. *Boreal Environment Research*, *18*(6), 488–502.
- Flener, C., Vaaja, M., Jaakkola, A., Krooks, A., Kaartinen, H., Kukko, A., et al. (2013). Seamless mapping of river channels at high resolution using mobile LiDAR and UAV-photography. *Remote Sensing (Basel)*, *5*(12), 6382–6407. <https://doi.org/10.3390/rs5126382>
- Fu, L., Alsdorf, D., Morrow, R., Rodriguez, E., & Mognard, N. (2012). *SWOT: The Surface Water And Ocean Topography mission* (JPL Publ. 12-05). Pasadena, CA: Jet Propulsion Laboratory.
- Garambois, P. A., & Monnier, J. (2015). Inference of effective river properties from remotely sensed observations of water surface. *Advances in Water Resources*, *79*, 103–120.
- Giustarini, L., Matgen, P., Hostache, R., Montanari, M., Plaza, D., Pauwels, V. R. N., et al. (2011). Assimilating SAR-derived water level data into a hydraulic model: A case study. *Hydrology and Earth System Sciences*, *15*(7), 2349–2365. <https://doi.org/10.5194/hess-15-2349-2011>
- Gleason, C. J., & Smith, L. C. (2014). Toward global mapping of river discharge using satellite images and at-many-stations hydraulic geometry. *Proceedings of the National Academy of Sciences of the United States of America*, *111*(13), 4788–4791. <https://doi.org/10.1073/pnas.1317606111>
- Han, B. S., & Endreny, T. A. (2014). River surface water topography mapping at sub-millimeter resolution and precision with close range photogrammetry: Laboratory scale application. *IEEE Journal of Selected Topics in Applied Earth Observations and Remote Sensing*, *7*(2), 602–608. <https://doi.org/10.1109/JSTARS.2014.2298452>
- Hilldale, R. C., & Raff, D. (2008). Assessing the ability of airborne LiDAR to map river bathymetry. *Earth Surface Processes and Landforms*, *33*(5), 773–783. <https://doi.org/10.1002/esp.1575>
- Jarrett, R. D. (1984). Hydraulics of high-gradient streams. *Journal of Hydraulic Engineering*, *110*(11), 1519–1539. [https://doi.org/10.1061/\(ASCE\)0733-9429\(1984\)110:11\(1519\)](https://doi.org/10.1061/(ASCE)0733-9429(1984)110:11(1519))
- Javernick, L., Brasington, J., & Caruso, B. (2014). Modeling the topography of shallow braided rivers using Structure-from-Motion photogrammetry. *Geomorphology*, *213*, 166–182. <https://doi.org/10.1016/j.geomorph.2014.01.006>
- Johnson, E. D., & Cowen, E. A. (2016). Remote monitoring of volumetric discharge employing bathymetry determined from surface turbulence metrics. *Water Resources Research*, *52*, 2178–2193. <https://doi.org/10.1002/2015WR017736>
- Kane, D. L., McNamara, J. P., Yang, D. Q., Olsson, P. Q., & Gieck, R. E. (2003). An extreme rainfall/runoff event in Arctic Alaska. *Journal of Hydrometeorology*, *4*(6), 1220–1228. [https://doi.org/10.1175/1525-7541\(2003\)004<1220:AEREIA>2.0.CO;2](https://doi.org/10.1175/1525-7541(2003)004<1220:AEREIA>2.0.CO;2)

- King, T. V., Neilson, B. T., Overbeck, L. D., & Kane, D. L. (2016). Water temperature controls in low arctic rivers. *Water Resources Research*, 52, 4358–4376. <https://doi.org/10.1002/2015WR017965>
- Kouraev, A. V., Zakharova, E. A., Samain, O., Mognard, N. M., & Cazenave, A. (2004). Ob' river discharge from TOPEX/Poseidon satellite altimetry (1992–2002). *Remote Sensing of Environment*, 93(1–2), 238–245. <https://doi.org/10.1016/j.rse.2004.07.007>
- Lammers, R. B., Shiklomanov, A. I., Vorosmarty, C. J., Fekete, B. M., & Peterson, B. J. (2001). Assessment of contemporary Arctic river runoff based on observational discharge records. *Journal of Geophysical Research: Atmospheres*, 106(D4), 3321–3334. <https://doi.org/10.1029/2000JD900444>
- Lane, S. N., Richards, K. S., & Chandler, J. H. (1994). Developments in monitoring and modelling small-scale river bed topography. *Earth Surface Processes and Landforms*, 19(4), 349–368. <https://doi.org/10.1002/esp.3290190406>
- Legleiter, C. J. (2015). Calibrating remotely sensed river bathymetry in the absence of field measurements: Flow Resistance Equation-Based Imaging of River Depths (FREEBIRD). *Water Resources Research*, 51, 2865–2884. <https://doi.org/10.1002/2014WR016624>
- Legleiter, C. J., Kinzel, P. J., & Nelson, J. M. (2017). Remote measurement of river discharge using thermal particle image velocimetry (PIV) and various sources of bathymetric information. *Journal of Hydrology*, 554, 490–506. <https://doi.org/10.1016/j.jhydrol.2017.09.004>
- Legleiter, C. J., Roberts, D. A., & Lawrence, R. L. (2009). Spectrally based remote sensing of river bathymetry. *Earth Surface Processes and Landforms*, 34(8), 1039–1059. <https://doi.org/10.1002/esp.1787>
- Legleiter, C. J., Roberts, D. A., Marcus, W. A., & Fonstad, M. A. (2004). Passive optical remote sensing of river channel morphology and in-stream habitat: Physical basis and feasibility. *Remote Sensing of Environment*, 93(4), 493–510. <https://doi.org/10.1016/j.rse.2004.07.019>
- Leopold, L. B., & Maddock, T. (1953). *The hydraulic geometry of stream channels and some physiographic implications*. Washington, DC: United States Government Publishing Office.
- Liu, G., Schwartz, F. W., Tseng, K.-H., & Shum, C. K. (2015). Discharge and water-depth estimates for ungauged rivers: Combining hydrologic, hydraulic, and inverse modeling with stage and water-area measurements from satellites. *Water Resources Research*, 51, 6017–6035. <https://doi.org/10.1002/2015WR016971>
- López, R., Barragán, J., & Colomer, M. À. (2007). Flow resistance equations without explicit estimation of the resistance coefficient for coarse-grained rivers. *Journal of Hydrology*, 338(1–2), 113–121. <https://doi.org/10.1016/j.jhydrol.2007.02.027>
- Lyon, J. G., Lunetta, R. S., & Williams, D. C. (1992). Airborne multispectral scanner data for evaluating bottom sediment types and water depths of the St Marys River, Michigan. *Photogrammetric Engineering and Remote Sensing*, 58(7), 951–956.
- Lyzenga, D. R. (1981). Remote sensing of bottom reflectance and water attenuation parameters in shallow water using aircraft and Landsat data. *International Journal of Remote Sensing*, 2(1), 71–82. <https://doi.org/10.1080/01431168108948342>
- Marcus, W. A., Legleiter, C. J., Aspinall, R. J., Boardman, J. W., & Crabtree, R. L. (2003). High spatial resolution hyperspectral mapping of in-stream habitats, depths, and woody debris in mountain streams. *Geomorphology*, 55(1–4), 363–380. [https://doi.org/10.1016/S0169-555X\(03\)00150-8](https://doi.org/10.1016/S0169-555X(03)00150-8)
- McClelland, J. W., Déry, S. J., Peterson, B. J., Holmes, R. M., & Wood, E. F. (2006). A pan-arctic evaluation of changes in river discharge during the latter half of the 20th century. *Geophysical Research Letters*, 33, L06715. <https://doi.org/10.1029/2006GL025753>
- McNamara, J. P., Kane, D. L., & Hinzman, L. D. (1998). An analysis of streamflow hydrology in the Kuparuk River basin, Arctic Alaska: A nested watershed approach. *Journal of Hydrology*, 206(1–2), 39–57. [https://doi.org/10.1016/S0022-1694\(98\)00083-3](https://doi.org/10.1016/S0022-1694(98)00083-3)
- Melcher, N. B., Costa, J. E., Haeni, F. P., Cheng, R. T., Thurman, E. M., Buursink, M., et al. (2002). River discharge measurements by using helicopter-mounted radar. *Geophysical Research Letters*, 29(22), 2084. <https://doi.org/10.1029/2002GL015525>
- Mersel, M. K., Smith, L. C., Andreadis, K. M., & Durand, M. T. (2013). Estimation of river depth from remotely sensed hydraulic relationships. *Water Resources Research*, 49, 3165–3179. <https://doi.org/10.1002/wrcr.20176>
- Neal, J., Schumann, G., Bates, P., Buytaert, W., Matgen, P., & Pappenberger, F. (2009). A data assimilation approach to discharge estimation from space. *Hydrological Processes*, 23(25), 3641–3649.
- Pan, F. F., Wang, C., & Xi, X. H. (2016). Constructing river stage-discharge rating curves using remotely sensed river cross-sectional inundation areas and river bathymetry. *Journal of Hydrology*, 540, 670–687. <https://doi.org/10.1016/j.jhydrol.2016.06.024>
- Pavelsky, T. M., Durand, M. T., Andreadis, K. M., Beighley, R. E., Paiva, R. C. D., Allen, G. H., et al. (2014). Assessing the potential global extent of SWOT river discharge observations. *Journal of Hydrology*, 519, 1516–1525. <https://doi.org/10.1016/j.jhydrol.2014.08.044>
- Peterson, B. J., Holmes, R. M., McClelland, J. W., Vorosmarty, C. J., Lammers, R. B., Shiklomanov, A. I., et al. (2002). Increasing river discharge to the Arctic Ocean. *Science*, 298(5601), 2171–2173. <https://doi.org/10.1126/science.1077445>
- Riggs, H. C. (1976). A simplified slope-area method for estimating flood discharges in natural channels. *Journal of Research of the U. S. Geological Survey*, 4, 285–291.
- Rosenfeld, J. S., Macdonald, S., Foster, D., Amrhein, S., Bales, B., Williams, T., et al. (2002). Importance of small streams as rearing habitat for coastal cutthroat trout. *North American Journal of Fisheries Management*, 22(1), 177–187. [https://doi.org/10.1577/1548-8675\(2002\)022<0177:IOSSAR>2.0.CO;2](https://doi.org/10.1577/1548-8675(2002)022<0177:IOSSAR>2.0.CO;2)
- Smith, L. C. (1997). Satellite remote sensing of river inundation area, stage, and discharge: A review. *Hydrological Processes*, 11(10), 1427–1439.
- Smith, L. C., Isacks, B. L., Bloom, A. L., & Murray, A. B. (1996). Estimation of discharge from three braided rivers using synthetic aperture radar satellite imagery: Potential application to ungauged basins. *Water Resources Research*, 32(7), 2021–2034.
- Stumpf, A., Augereau, E., Delacourt, C., & Bonnier, J. (2016). Photogrammetric discharge monitoring of small tropical mountain rivers: A case study at Rivière des Pluies, Réunion Island. *Water Resources Research*, 52, 4550–4570. <https://doi.org/10.1002/2015WR018292>
- Su, H., Liu, H., & Heyman, W. D. (2008). Automated derivation of bathymetric information from multi-spectral satellite imagery using a non-linear inversion model. *Marine Geodesy*, 31(4), 281–298. <https://doi.org/10.1080/01490410802466652>
- Vetter, M., Höfle, B., Hollaus, M., Gschöpf, C., Mandlbürger, G., Pfeifer, N., et al. (2011). Vertical vegetation structure analysis and hydraulic roughness determination using dense ALS point cloud data—A voxel based approach. *International Archives of Photogrammetry, Remote Sensing and Spatial Information Sciences*, 38, 5.
- Watanabe, Y., & Kawahara, Y. (2016). UAV photogrammetry for monitoring changes in river topography and vegetation. *Procedia Engineering*, 154, 317–325. <https://doi.org/10.1016/j.proeng.2016.07.482>
- Westaway, R. M., Lane, S. N., & Hicks, D. M. (2003). Remote survey of large-scale braided, gravel-bed rivers using digital photogrammetry and image analysis. *International Journal of Remote Sensing*, 24(4), 795–815. <https://doi.org/10.1080/01431160110113070>
- Wilson, M. D., Durand, M., Jung, H. C., & Alsdorf, D. (2015). Swath-altimetry measurements of the main stem Amazon River: Measurement errors and hydraulic implications. *Hydrology and Earth System Sciences*, 19(4), 1943–1959. <https://doi.org/10.5194/hess-19-1943-2015>
- Yoon, Y., Durand, M., Merry, C. J., Clark, E. A., Andreadis, K. M., & Alsdorf, D. E. (2012). Estimating river bathymetry from data assimilation of synthetic SWOT measurements. *Journal of Hydrology*, 464–465, 363–375. <https://doi.org/10.1016/j.jhydrol.2012.07.028>
- Yoon, Y., Garambois, P.-A., Paiva, R. C. D., Durand, M., Roux, H., & Beighley, E. (2016). Improved error estimates of a discharge algorithm for remotely sensed river measurements: Test cases on Sacramento and Garonne Rivers. *Water Resources Research*, 52, 278–294. <https://doi.org/10.1002/2015WR017319>